

3D-Informed Targeting of the Trop-2 Signal-Activation Site Drives Selective Cancer Vulnerability



Emanuela Guerra^{1,2}, Marco Trerotola^{1,2}, Valeria Relli¹, Rossano Lattanzio¹, Romina Tripaldi¹, Martina Ceci^{1,2}, Khoulood Boujnah³, Ludovica Pantalone¹, Andrea Sacchetti¹, Kristina M. Havas¹, Pasquale Simeone¹, Nicole Travali³, Patrizia Querzoli⁴, Massimo Pedriali⁵, Pietro Roversi^{6,7}, Manuela Iezzi⁸, Nicola Tinari², Laura Antolini⁹, and Saverio Alberti⁵

ABSTRACT

Next-generation Trop-2–targeted therapy against advanced cancers is hampered by expression of Trop-2 in normal tissues. We discovered that Trop-2 undergoes proteolytic activation by ADAM10 in cancer cells, leading to the exposure of a previously inaccessible protein groove flanked by two N-glycosylation sites. We designed a recognition strategy for this region, to drive selective cancer vulnerability in patients. Most indiscriminating anti-Trop-2 mAbs recognize a single immunodominant epitope. Hence, we removed it by deletion mutagenesis. Cancer-specific, glycosylation-prone mAbs were selected by ELISA, bio-layer interferometry, flow cytometry, confocal microscopy for differential binding to cleaved/

activated, wild-type and glycosylation site–mutagenized Trop-2. The resulting 2G10 mAb family binds Trop-2–expressing cancer cells, but not Trop-2 on normal cells. We humanized 2G10 by state-of-the-art complementarity determining region grafting/re-modeling, yielding Hu2G10. This antibody binds cancer-specific, cleaved/activated Trop-2 with $K_d < 10^{-12}$ mol/L, and uncleaved/wtTrop-2 in normal cells with $K_d 3.16 \times 10^{-8}$ mol/L, thus promising an unprecedented therapeutic index in patients. *In vivo*, Hu2G10 ablates growth of Trop-2–expressing breast, colon, prostate cancers, but shows no evidence of systemic toxicity, paving the way for a paradigm shift in Trop-2–targeted therapy.

Introduction

Trop-2 (AC: P09758), also known as EGP-1, T16, MR23, MR54, is a type-I transmembrane protein, encoded by the tumor-associated calcium signal transducer 2 (*TACSTD2/MIS1/GA733-1*) gene (1–3), a retrotransposon of the *TROP1/TACSTD1/EPCAM* gene (2, 4). The extracellular domain of human Trop-2 (ECD, residues 27–274) encompasses a cysteine-rich N-terminal region, which hosts a GA733 type 1 motif (residues 27–69) and a thyroglobulin type-1 domain (residues 70–148), followed by a C-terminal domain devoid of cysteines (residues 149–274; ref. 1). A single transmembrane helix connects the ECD to a 26-amino acid (AA) intracellular tail, which contains a HIKE motif (5) and two PKC phosphorylation sites at Ser303 (6) and Ser322 (7) and drives downstream Ca^{2+} , PKC, and AKT signaling (8–10).

Trop-2 induces tumor and cancer stem cell growth (11–14). Upregulation of Trop-2 has been associated with poor prognosis of pancreatic, gastric, ovarian, lung, and colorectal cancers (15, 16), indicating a key role of this molecule in tumor progression (12–14).

Most anti-Trop-2 mAbs, including MOv16 (17), cAR47A6.4.2 (18), 162–46.2 (17), Pr1E11 (19), and AbT16 (14), all bind to the same immunodominant epitope (17) located within the D146-L274 region (19). RS7, the parental mAb for Sacituzumab Govitecan (SG; TRODELVY, IMMU-132; ref. 20), which was approved by the FDA for patients with metastatic triple-negative breast cancer (TNBC; refs. 21, 22) and urothelial carcinomas (23), binds a corresponding region (24). The E1 mAb, which was designed using more recent technology, was still found to bind the same immunodominant epitope as the RS7, AbT16, and 162–46.2 mAb (14).

¹Laboratory of Cancer Pathology, Center for Advanced Studies and Technology (CAST), “G. d’Annunzio” University of Chieti-Pescara, Chieti, Italy.

²Department of Medical, Oral and Biotechnological Sciences, “G. d’Annunzio” University of Chieti-Pescara, Chieti, Italy.

³Unit of Medical Genetics, Department of Biomedical Sciences - BIOMORF, University of Messina, Messina, Italy.

⁴Section of Anatomic Pathology, University of Ferrara, Ferrara, Italy.

⁵Department of Pathology, Ferrara Hospital, Ferrara, Italy.

⁶Italian National Research Council (CNR), Institute of Agricultural Biology and Biotechnology (IBBA-CNR), Milano, Italy.

⁷Leicester Institute of Chemical and Structural Biology and Department of Molecular and Cell Biology, University of Leicester, Leicester, England, United Kingdom.

⁸Department of Neurosciences, Imaging and Clinical Sciences, Center for Advanced Studies and Technology (CAST), “G. d’Annunzio” University of Chieti-Pescara, Chieti, Italy.

⁹Center for Biostatistics, Department of Clinical Medicine, Prevention and Biotechnology, University of Milano-Bicocca, Monza, Italy.

Current address for Valeria Relli: Oncologia Medica, Azienda Ospedaliero-Universitaria di Bologna, Bologna, Italy; Center of Applied Biomedical Research, S. Orsola-Malpighi University Hospital, Bologna, Italy.

Current address for Rossano Lattanzio: Department of Innovative Technologies in Medicine and Dentistry, Center for Advanced Studies and Technology (CAST), University “G. d’Annunzio” University of Chieti-Pescara, Chieti, Italy.

Current address for Andrea Sacchetti: Josephine Nefkens Institute, Erasmus MC, Rotterdam, the Netherlands.

Current address for Kristina M. Havas: FIRC Institute of Molecular Oncology (IFOM), Milan, Italy.

Current address for Pasquale Simeone: Department of Medicine and Aging Sciences, “G. d’Annunzio University” of Chieti-Pescara, Chieti, Italy; Laboratory of Cytomorphology, Center for Advanced Studies and Technology (CAST), “G. d’Annunzio” University of Chieti-Pescara, Chieti, Italy.

E. Guerra and M. Trerotola contributed equally as co-first authors of this article.

Corresponding Author: Saverio Alberti, BIOMORF, University of Messina, via Consolare Valeria, Messina 98125, Italy. E-mail: salberti@unime.it

Mol Cancer Ther 2023;22:790–804

doi: 10.1158/1535-7163.MCT-22-0352

©2023 American Association for Cancer Research

The Rinat-Pfizer PF-06664178 anti-Trop-2 ADC was also shown to bind the Trop-2 ECD immunodominant epitope, at AA 152–206 and 209–274. Despite early promise, PF-06664178 was ultimately dropped because of excess toxicity and modest antitumor activity (25). As indicated, SG/TRODELVY/IMMU-132 shows an impact in patients with TNBC (21, 22). Corresponding promise was shown in patients with additional types of Trop-2-expressing cancers. However, the SG half-life in plasma is 11 to 14 hours (26). SG induces limiting side effects (21, 22), such as neutropenia and diarrhea, which appear linked to ineffective retention of its SN38 payload in the circulation (20, 27).

Limited efficacy versus difficult-to-manage toxicity severely plague current anti-Trop-2-targeted antibody therapy. In this context, a major stumbling block for next-generation therapeutic strategies remains the broad expression of Trop-2 in normal tissues (28). We discovered that activation of Trop-2 for driving tumor progression requires proteolytic activation by ADAM10 in cancer cells (14, 16). Importantly, Trop-2 cleavage by ADAM10 was found not to occur in normal tissues (14, 16).

This finding provided the potential for a cancer-only Trop-2-targeting therapeutic strategy. A structure/function-instructed analysis was conducted to identify the cleavage-activated, signal-triggering region of Trop-2. Accessibility-directed activation-site recognition was then carried out to target cancer-exposed sites in order to exploit this unique cancer vulnerability in patients (29, 30).

Materials and Methods

Trop-2 structure analysis

Initially, a homology model for the ECD thyroglobulin-like repeat was constructed over the p41 splice variant of the MHC class II-associated invariant chain (PDB ID 1ICF, chain I; refs. 14, 31). The mature portion of human Trop-2, residues 27–323 (Uniprot P09758 (TACD2_HUMAN) was subsequently modelled as a cis-dimer analogous to the dimer in the crystal of human Trop-1/EpCAM [PDB ID 4MZV (32), 45% sequence identity over 240 residues (1, 4)], and the dimer in the Nuclear Magnetic Resonance (NMR)-derived model of the transmembrane region of the rat p75 protein [PDB ID 4MZV, residues 278–298, 30% sequence identity over 21 residues (33)]. These protein models were used as templates. The cytoplasmic domain of human Trop-2, portion 299–323, was inherited from the NMR structure of the C-terminus of Trop-2 (PDB ID 2MAE; ref. 34). The region 270–277 in our homology model has arbitrary structure in that no good homologous model is available (the Trop-1/EpCAM C-terminus 270–274 likely needs reorientation to point toward the membrane). Twenty models were made, and the best-fitting one was selected; it preserved the intramembrane helical dimer observed in rat p75.

Once the structures of the human Trop-2 ECD were published (24, 35), the analysis was validated over the crystal structure in PDB ID 7PEE (35). Structure files were from the Research Collaboratory for Structural Bioinformatics Protein Data Bank (RCSB PDB; RRID:SCR_012820). Swiss-PdbViewerDeepView4.0 (RRID:SCR_013295) and PyMol (RRID:SCR_000305) were used for graphic rendering of the 3D structures. N-glycosylation was added to Asn residues N33, N120, N168, and N208 using the GlyProt server (ref. 36; www.glycosciences.de/modeling/glyprot/php/main.php). The list of residues at the interface between the N-terminal cleaved portion, the Trop-2 transmembrane portion, and the area buried in this interface were computed at the PISA server (www.ebi.ac.uk/pdbe/pisa/; www.ebi.ac.uk/pdbe/prot_int/pistart.html).

Anti-ADAM10 cleaved/activated-trop-2 murine mAb generation

Deletion mutants of Trop-2 ECD were generated from mammalian tumor cell transfectants (human 293, MCF-7, murine L cells), baculovirus-expressing insect cells, yeast cells and *Escherichia coli*, purified, and used as immunogen in Balb/c mice. Individual hybridoma clones were generated and screened for production of mAb specific to cell surface-expressed Trop-2 deletion mutants by ELISA on transfected cell monolayers. The 10 top-binding hybridomas were further selected for reactivity against living L cells transfected with full-length wild-type (WT) Trop-2 by flow cytometry. Five *in vivo* Trop-2-reactive hybridomas (1A9, 1B4, 2EF, 2G10, 4F6) were further assayed for binding to L cells transfected with Trop-2 deletion mutants, to identify their target regions. mAb isotype was determined by ELISA. The anti-Trop-2 AbT16 and AR47A6.4.2 (International Depository Authority of Canada, Winnipeg, MB) and the irrelevant mAb p181Bg were used as Trop-2-binding *versus* Trop-2-nonbinding control mAb, respectively. mAb isotyping identified 2EF as IgG2b/k and 2G10 as IgG2a/k. The 2EF-secreting hybridoma was cloned twice, to 2EF.22.21 to increase stability of mAb production.

DNA transfection

Cells were transfected with DNA (37) in Lipofectamine 2000 or LTX (Invitrogen) following the manufacturer's instructions. Stable transfectants were selected in G-418-containing medium.

Elisa

ELISA assay plates were coated overnight at 4°C with 100 µL/well of 1 µg/mL recombinant human Trop-2-IgFc chimera protein (rhTROP-2; R&D, catalog No. 650-T2-100), in 0.2 mol/L sodium carbonate buffer (pH 9.4). Well surfaces were blocked with 300 µL/well of blocking buffer (2% skim milk in PBS, 0.05% Tween-20) for 30 minutes at room temperature. The plates were washed twice with wash buffer (PBS, 0.05% Tween-20). Purified antibodies or supernatants were added to the plates at serial threefold dilutions, starting from 5 to 10 µg/mL, 100 µL/well. All dilutions were performed in blocking buffer. Antibody-containing plates were incubated for 1 hour at room temperature. The plates were then washed three times with wash buffer. Antibody binding was revealed with 100 µL/well of a 1:2,000 dilution of goat anti-human kappa-HRP (SouthernBiotech, catalog No. 2060-05) in blocking buffer, incubated for 30 minutes at room temperature, and washed four times with wash buffer. Horseradish peroxidase activity was revealed with 100 µL/well ABTS substrate (AMRESCO, Solon, OH), activated with 20-µL 30% H₂O₂ per 10-mL ABTS solution. The reaction was stopped with 100 µL per well 2% oxalic acid. Absorbance was read at 405 nm.

Flow cytometry

Cell staining for flow cytometry was performed as described (38). Fluorescence analysis and cell sorting were carried out on fluorescence-activated cell analyzers and sorters (FACS Aria III, Canto II, Becton Dickinson, Sunnyvale, CA) after enrichment for expressing transfectants with Magnetic Cell Sorting-MACS from Miltenyi Biotec GmbH (Germany). To improve signal-to-noise ratios and the detection of transfectants stained with FITC-mAb, subtraction of cell autofluorescence and displacement of FITC-stained cells in the red channel were performed as described (39, 40). All Trop-2 transfectants were selected for expression levels comparable with those of endogenously expressing human cancer cells (8, 41). mAb were conjugated to Alexa488, 546 or 633 (Life Technologies, Carlsbad, CA) for direct cell staining.

Immunofluorescence and confocal microscopy

Cells plated on glass coverslips were fixed with 4% paraformaldehyde in PBS for 20 minutes. Permeabilization and blocking were performed in medium with 10% FCS and 0.1% saponin. Live cells on glass coverslips were stained in medium with 10% FCS at 37°C for 5 minutes and fixed after staining. Slides were analyzed by immunofluorescence (IF) with the LSM-510 META and LSM800 (Zeiss) confocal microscopes. Three laser beams were used, emitting at wavelengths of 488 nm (argon ion laser, 200 mW, 2%–5% applied laser power), and 543 nm (diode laser, 1 mW, 50%–100% applied laser power), 633 nm (diode laser, 5 mW, 50% applied laser power). HFT 488/543 or 488/543/633 beam-splitters were used, as needed for multicolor fluorochrome-conjugated antibody analysis, with band-pass emission filters 505 to 550 nm (green channel); long-pass 560 nm (for two-color analysis), or band-pass 560 to 615 nm (for three-color analyses) in the orange channel; or long-pass 650 nm in the deep-red channel. HFT 488/543 and a band-pass of 505- to 550-nm filter in the green channel were used for EGFP detection. Images were acquired in Multiplex mode, that is, via sequential, separate acquisition of individual laser lines/fluorescence channels to prevent cross-channel fluorescence spill over. Detector gains of ≤ 770 V were applied to minimize electronic noise. Amplifier gains were $\leq 2.8\times$. Images were acquired as 1024 \times 1024 pixel format, except where indicated. Images were captured as averages of four sequential acquisitions, using a 40 \times /1.2, 63 \times /1.4 oil DIC objective (Plan-Apochromat; Zeiss).

Hu2G10 generation

Construction of chimeric 2G10 IgG1/ κ -antibody. Total RNA was extracted from 2G10 hybridoma cells using TRIzol according to the manufacturer's instructions and used as template for the synthesis of the heavy- and light-chain variable region (VH and VL respectively) full-length cDNAs via nested RT-PCR, using the SMARTer RACE cDNA Amplification Kit with the universal primers provided and the following specific primers:

2G10 VH R: reverse 5'-GCCAGTGGATAGACCGATGG-3'
 2G10 VL F: forward 5'-ACCAGCACTGATATTGATG-3'
 2G10 VL R: reverse 5'-CTCCCTAACACTCATTCCTGTTGAAGC-3'
 2G10-VL-R3: reverse 5'-CGTGTACGGCAAGTTATCAC-3'
 The 2G10 VH e VL were sequenced and PCR amplified with the primers below, to include splice donor signals from the mouse germline JH4 and J κ 1 respectively:
 2G10 VH CH-F forward: 5'-GCAACTAGTACCACCATGGAATGGAAGTGGGTC-3'
 2G10 VH CH-R reverse: 5'-GGGAAGCTTGAGAGGCCATTCTTACCTGAGGAGACGTGACTGAGGT-3'
 2G10 VL CH-F forward: 5'-GCTGCTAGCACCACCATGTTCTCACTAGCTCTTCTCC-3'
 2G10 VL CH-R reverse: 5'-CGAGAATCTTTGGATTCTACTTACGTTTGATTCCAGCTTGTC-3'

The PCR fragments were purified and cloned as exons under a CMV promoter upstream of human G1 and κ constant regions, to obtain the pCh2G10 vector for mammalian expression of the chimeric 2G10 IgG1/ κ antibody (Ch2G10).

2G10 antibody humanization. The human Ig VH sequence AC: X65888.1 and VL sequence AY043146.1 were chosen as acceptors for humanization. The complementarity determining regions (CDRs) sequences of 2G10 VH and VL were transferred to the corresponding

positions of the human sequences and humanized according to predicted 3D structures. Two VH and eight VL were obtained as optimized humanized versions. Combinatorial expression vectors were transiently transfected into the human embryonic kidney cell line HEK293 using Lipofectamine 2000. Antibodies were purified from cell culture supernatants by protein-A affinity chromatography and Trop-2 binding was measured by ELISA as described. Vectors expressing the two VH/VL combinations that gave the highest binding affinities, comparable with Ch2G10 (VH1 and VL3, named pHu2G10-5; VH2 and VL3, named pHu2G10-6; patent application WO201608765) were then transfected into mouse myeloma NS-0 cells by electroporation and seeded as single-cell clones in 96-well plates. Culture supernatants were assayed for antibody production by sandwich ELISA as described. Stable transfectants producing high levels of the corresponding antibodies were adapted to grow in serum-free Hybridoma SFM medium (Life Technologies). Antibodies were purified from supernatants by protein-A affinity chromatography.

Stable hamster CHO-K1 transfectants were also obtained by electroporation and single-cell selection as described above and adapted to grow in serum-free SFM4CHO medium (HyClone). Higher yields of Hu2G10 mAb were produced in CHO-K1 cells, hence these were chosen as production hosts for the following steps.

Antibody-dependent cellular cytotoxicity assay

Jurkat NF- κ B/NFAT [antibody-dependent cellular cytotoxicity (ADCC) Reporter Bioassay, Core Kit, catalog No. G7010, Promega] was used as effector/reporter cells. MCF-7 breast cancer cells were used as targets. Briefly, MCF-7 target cells (25,000 cells/well) were seeded in a white, flat-bottom 96-well assay plate (catalog No. 655001, Corning) in 100- μ L RPMI medium with 10% FBS and 1% P/S. The day after, 37.6 μ g of purified Hu2G10 mAb was diluted in 200- μ L ADCC assay buffer (96% RPMI1640 with L-glutamine, 4% low IgG FBS). Fivefold serial dilutions were prepared in ADCC assay buffer for charting a dose-response curve. The medium was removed from the assay plate and 25 μ L of each mAb dilution was added to different wells of the assay plate. Three nonclustered replica wells were arranged for each mAb dilution, with negative controls not receiving mAb. Jurkat NF- κ B/NFAT effector/reporter cells were then added to each well (75,000 cells/well in 25 μ L of ADCC assay buffer; effector to target cell ratio, E:T = 3:1). After 17 hours at 37°C, 5% CO₂, the plate was equilibrated at room temperature, 75 μ L of Bio-Glo Luciferase Assay Reagent (Catalog No. G7941, Promega) was added to each well. After 5 minutes of incubation, the plate was read in a Veritas microplate luminometer (Turner Biosystems), with 0.5 seconds integration time. Luminescence values were plotted against the Log₁₀ of mAb concentration and the mAb EC₅₀ was calculated.

ADCC was also assessed using fresh human peripheral blood mononuclear cells (PBMCs) as effectors and impedance-based real-time analysis to measure target cell death (42) on an iCELLigence Real Time Cell Analyzer (Acea Biosciences) system. PBMCs were isolated from EDTA-blood from healthy donors by Ficoll-hypaque density-gradient centrifugation, assessed for vitality by Trypan blue counting, and cultured overnight at 1×10^6 to 2×10^6 cells/mL. Cells to be used for ADCC assessment were collected and checked for vitality. Batches with overnight loss of vitality <5% were resuspended in assay medium (complete RPMI with IL2 100 u/mL) and added at a ratio of 10:1 to monolayers of unlabelled target cells seeded 24 hours earlier in 16-well plates with golden electrodes as impedance sensors. Immediately after, the Hu2G10 mAb was added to each well at a final concentration of

10 µg/mL. Control wells received only PBMCs and no antibody. Plates were maintained in a humidified incubator at 37°C and 5% CO₂. Cell death was directly measured in real-time by impedance decrease, consequent to target cell detachment. Impedance data were collected every 3 minutes over a time span of 10 hours.

IHC

IHC of normal and neoplastic human tissues was performed as previously described (43). Briefly, specimens were fixed in phosphate-buffered formalin, pH 7.2 and embedded in paraffin. Five-micrometer sections were mounted on silanized slides, deparaffinized, and rehydrated through graded alcohols to water. Endogenous peroxidase activity was eliminated by incubation with 3% H₂O₂ for 5 minutes. Antigen retrieval was performed by microwave treatment at 750 W for 10 minutes in 1 mol/L urea buffer pH 8.0.

Sections were incubated for 30 minutes with the 162–46.2 anti-Trop-2 mAb (ATCC clone HB187) ascites at 1:500 dilution or the AF650 anti-Trop-2 goat pAb (R&D Systems). To control for non-specific reactivity, the specific primary antibodies were replaced with nonimmune serum or with isotype-matched immunoglobulins (DAKO). Anti-mouse (K4001, EnVision kit; DAKO) and anti-goat (K0679, LSAB kit; DAKO) secondary pAbs were used for signal amplification, as appropriate. Slides were washed in TBS-Tween 20 and incubated for 10 minutes in 3,3'-diaminobenzidine (DAKO). Counterstaining was performed with hematoxylin. Slides were mounted with Immunomount (Shandon).

Trop-2 expression was quantified by two independent observers as percentage of stained cells and as intensity of staining. An IHC score (H-score) was obtained (range, 0 to 12). Five classes of expression prevalence were categorized: 0 (0% of positive cells), 1 (<10% of

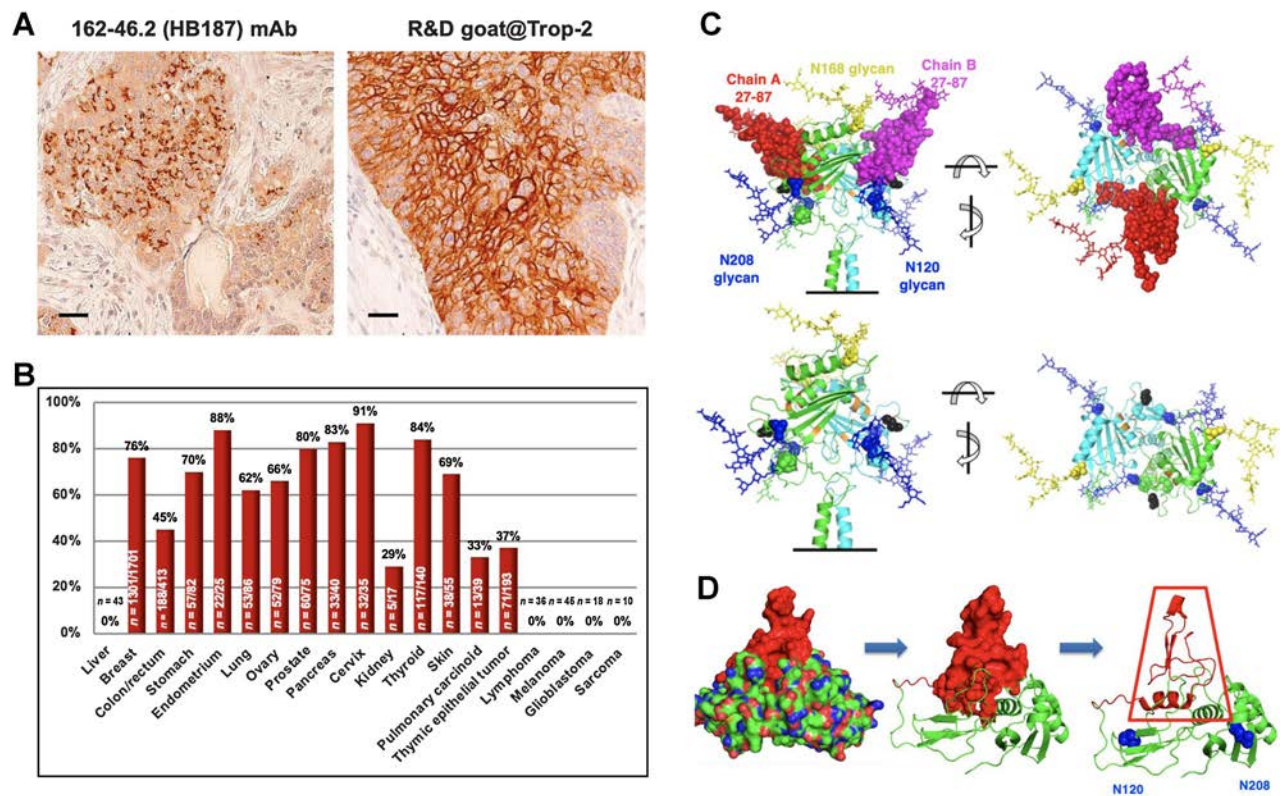


Figure 1.

The Trop-2 protein target in cancer. **A**, Trop-2 protein expression in cancer. IHC analysis of Trop-2 protein expression in human breast cancer samples. Left, Staining was performed with the 162–46.2 (HB187) murine mAb. Reactivity is prominent against intracellular Trop-2 deposits (43). Right, Staining was performed with the AF650 anti-Trop-2 goat polyclonal antibody. Prevalent reactivity against the cancer cell-membrane Trop-2-activated form was observed (43). Bars = 30 µm. **B**, Frequency of Trop-2 expression in human tumors. The tumor classes analyzed are listed on the X-axis. The height of the red bars is in proportion to the frequency of expression of Trop-2 (overall frequency on top of the bar). Absolute numbers of cases analyzed are listed within each frequency bar. **C** and **D**, 3D structure of Trop-2. **C**, Side and top (i.e., extracellular) views of the model of a human Trop-2 dimer (35), truncated in the middle of the transmembrane helices (horizontal black bar). As indicated by the arrows, the two views are related by a 90° horizontal rotation. A black circle and a black rectangle surround the groove between the glycans at N120 and N208 that becomes more accessible upon ADAM10 cleavage and rearrangement of the N-terminal ADAM10-cleaved subunit. Trop-2 molecules in the dimer are in green/cyan ribbons. Residues N120 and N208 are in blue spheres with the N-glycans at these sites in blue sticks. The N168 residue is in yellow spheres and its N-glycan is in yellow sticks. The two N-terminal ADAM10-cleaved subunits (AA 27–87) are in red/magenta spheres. The N33-linked glycans on this portion of the molecule are also in red/magenta sticks. The C73–C108 disulfide bridge that tethers the ADAM10-cleaved subunit to the rest of the protein is in black spheres. The groove residues forming salt bridges or hydrogen bonds with the removed ADAM10-cleaved subunits are in orange (footprint residues T88, G112, D221, Y224, Y225, E233, L235, Q237, Y260). Residue C108 (disulfide bonded to Cys 73 in the small cleaved subunit) is also part of the same groove region but is represented in black spheres in both panels. Top, Pre-cleavage Trop-2 dimer model. Bottom, Post-cleavage Trop-2 dimer model, with a possible novel orientation of the two N-terminal small subunits (AA 27–87) following ADAM-10 cleavage, preserving the C73–C108 disulphide bridge. **D**, Full-length Trop-2 ECD. The N-terminal subunit is in red. Surface sphere models versus ribbon diagrams are provided for clarity.

positive cells), 2 (10%–50% of positive cells), 3 (50%–80% of positive cells), and 4 (>80% of positive cells). An intensity score classified average intensity of positive cells as 1 (weak staining), 2 (moderate staining), or 3 (strong staining). The positivity and intensity scores were then multiplied to obtain a final H-score that ranked tumors for overall expression of Trop-2.

Experimental tumors

Transformed cell lines and *TROP-2* transfectants (37) were injected subcutaneously (5×10^6 to 10×10^6 cells) into 8-week-old female athymic CD1-Foxn1 nu/nu mice (Charles River Laboratories, RRID:

IMSR_CRL:086). The tumor longest/shortest diameters (D/d) were measured every 5 to 7 days. Tumor volumes were calculated as for an ellipsoid ($D \times d^2/2$; ref. 16). Treatment with anti-Trop-2 or irrelevant (p181bg) mAb was performed by weekly intraperitoneal administration of 800 $\mu\text{g}/\text{mouse}$ of antibody in PBS, for 4 weeks starting from the day of the inoculation.

Study approval

Procedures involving animals and their care were conducted in compliance with institutional guidelines, national laws, and international protocols (D.L. No.116, G.U., Suppl. 40, Feb.18, 1992;No.

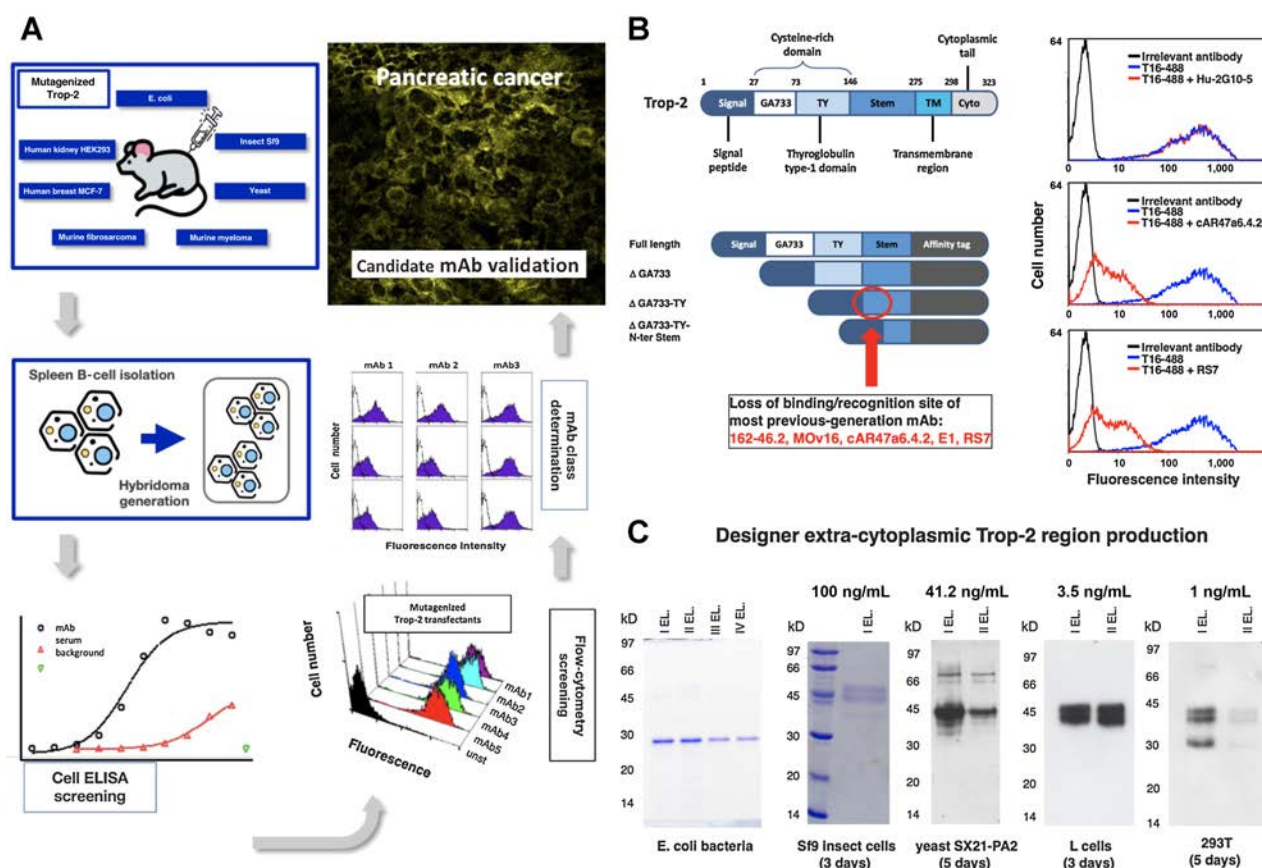


Figure 2. Generation and screening of mAb targeting cancer-activated Trop-2. **A**, Flow-chart of the generation strategy of cancer-selective anti-Trop-2 mAbs. Affinity-purified multi-phyla-derived Trop-2 immunogens were coinjected in Balb-C mice, from which hybridomas were generated as described. Hybridoma clone culture supernatants were screened by ELISA for mAb reactivity, using deletion mutant Trop-2-expressing transfectants as targets. Positive clones were then screened against native Trop-2 by flow cytometry. Native Trop-2-binding mAbs were assigned to homogeneous groups by cross-competition assays. Cancer reactivity was validated by multiplex IF analyses on frozen tumor tissue sections. **B**, Immunodominant recognition of Trop-2 [modified from (19)]. Left, Trop-2 schematics with indication of the different structural domains along the molecule; residue numbering is according to NP_002344.2. Numbers indicate boundary AA residues. Bottom, Trop-2 deletion mutant schematics; structural domains that were retained in each mutant are color-coded according to the full-length molecule. Right, Flow-cytometry analysis of competition assays versus immunodominant-epitope-binding mAb. KM12SM/Trop-2 transfectants were stained with the Alexa488-labelled benchmark AbT16 mAb (17), either alone (blue profiles) or coincubated with a 10-fold excess of unlabeled anti-Trop-2 mAb, as indicated (red profiles). RS7 (55) and AR47A6.4.2 (18) efficiently competed out AbT16, whereas 2G10 did not, indicating recognition of a different epitope. An irrelevant antibody was used as negative control (black solid-line profiles). **C**, Trop-2 recombinant protein immunogens. *E. coli*: the Trop-2 ECD synthesis was induced by IPTG and purified by 6His tag/Ni-NTA affinity chromatography, under denaturing conditions in 6M urea/guanidinium; purified Trop-2 showed the expected 29 kD mw as a deglycosylated form. Yeast: The S150-PA1 strain expresses gene the PDII disulfide-isomerase, which catalyzes the rearrangement of intrachain and interchain disulfide bonds, for native structure folding. The SX21-PA2 expresses the PDII gene and TRX2 (thioredoxin II), for improved disulfide bond reduction and rearrangement. Sf9, L, 293T cells were allowed to reach confluency in complete medium, then shifted to serum-free medium for the indicated time. Supernatants were collected and proteins were precipitated with saturated ammonium sulfate. Trop-2 variants were purified under non-denaturing conditions via 6His tag/Ni-NTA affinity chromatography. Sequential elutions were performed with NaCl step-gradients as described. The amount of secreted Trop-2 in each model system is indicated.

8, G.U., July, 1994; UKCCCR Guidelines for the Welfare of Animals in Experimental Neoplasia; EEC Council Directive 86/609, OJ L 358. 1, Dec.12, 1987; Guide for the Care and Use of Laboratory Animals, United States National Research Council, 1996), following approval by the Italian Ministry of Health (No. 723/2015-PR) and by the Animal Protection Committee of the Beijing Experimental Animal Center (Research Proposal Approval, June 30, 2015). Studies on human samples were approved by the Italian Ministry of Health (RicOncol RF-EMR-2006-361866, 2006).

Statistical analysis

The χ^2 test was used for comparison of errors between experimental data and fitted curves in Octet binding assays. Two-tailed Fisher exact tests were used to compare protein expression levels in normal *versus* tumor samples. EC₅₀ values were calculated from dose-response data fitted to a 4-parameter-logistic nonlinear regression model. Spearman nonparametric correlation coefficients were computed for protein expression levels in human cancer samples. ANOVA (44) and *t* test

implementing a *post hoc* Bonferroni correction were used to comparatively assess tumor growth curves. Data were analyzed using Sigma Stat (SPSS RRID:SCR_002865) and GraphPad Prism (RRID: SCR_002798).

Data availability

All relevant data are included in this article. The sequence data of the Hu2G10-5 and Hu2G10-6 are described in the patent application WO2016087651 available at <https://patents.google.com/patent/WO2016087651A1/en>.

Results

3D-informed recognition of cancer-specific ADAM10-processed Trop-2

Large-scale IHC analysis of human tumors (3,132 cases) was conducted with the benchmark 162-46.2 mAb and with the R&D goat pAb, which recognizes the activated form of Trop-2 (43). Cancers

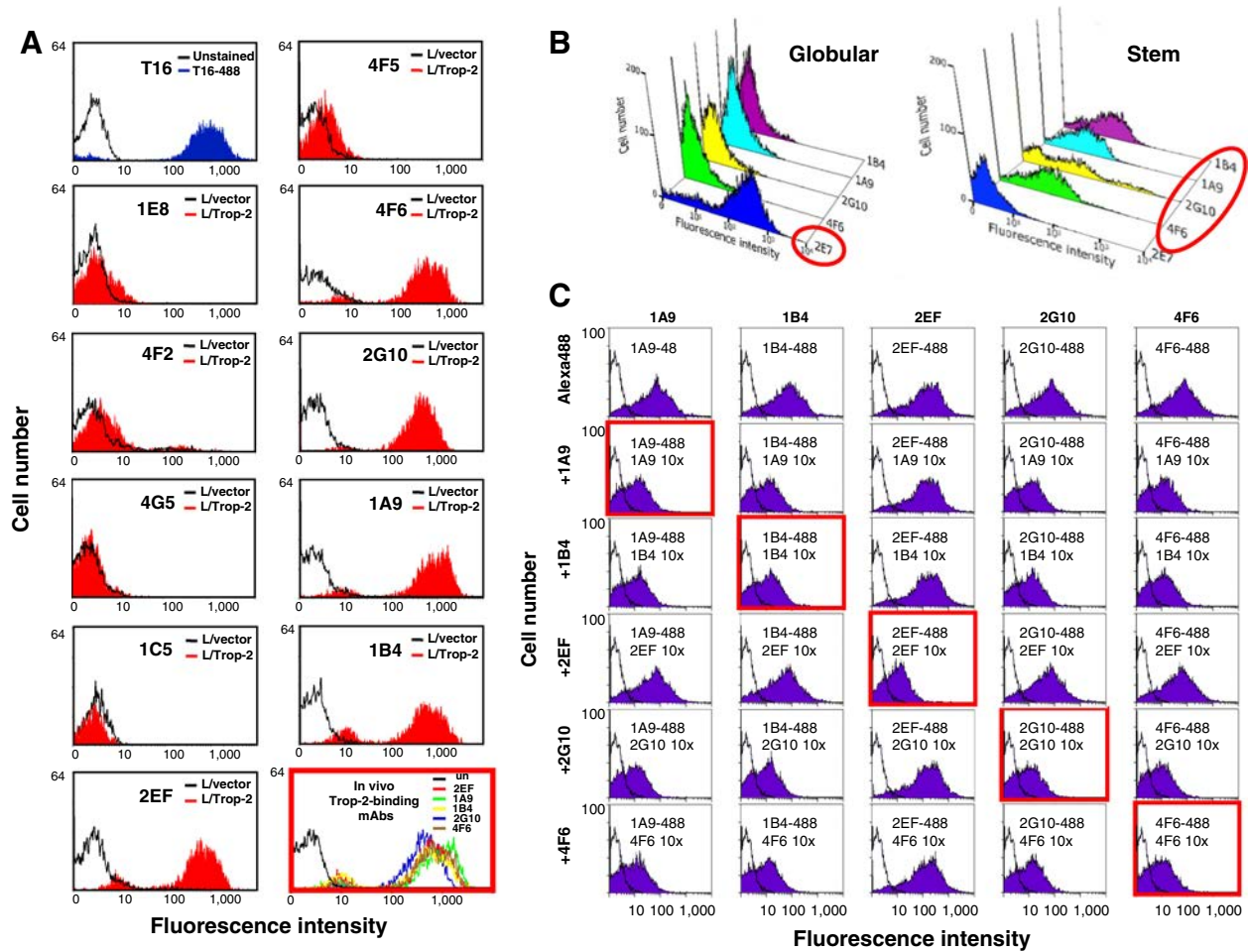
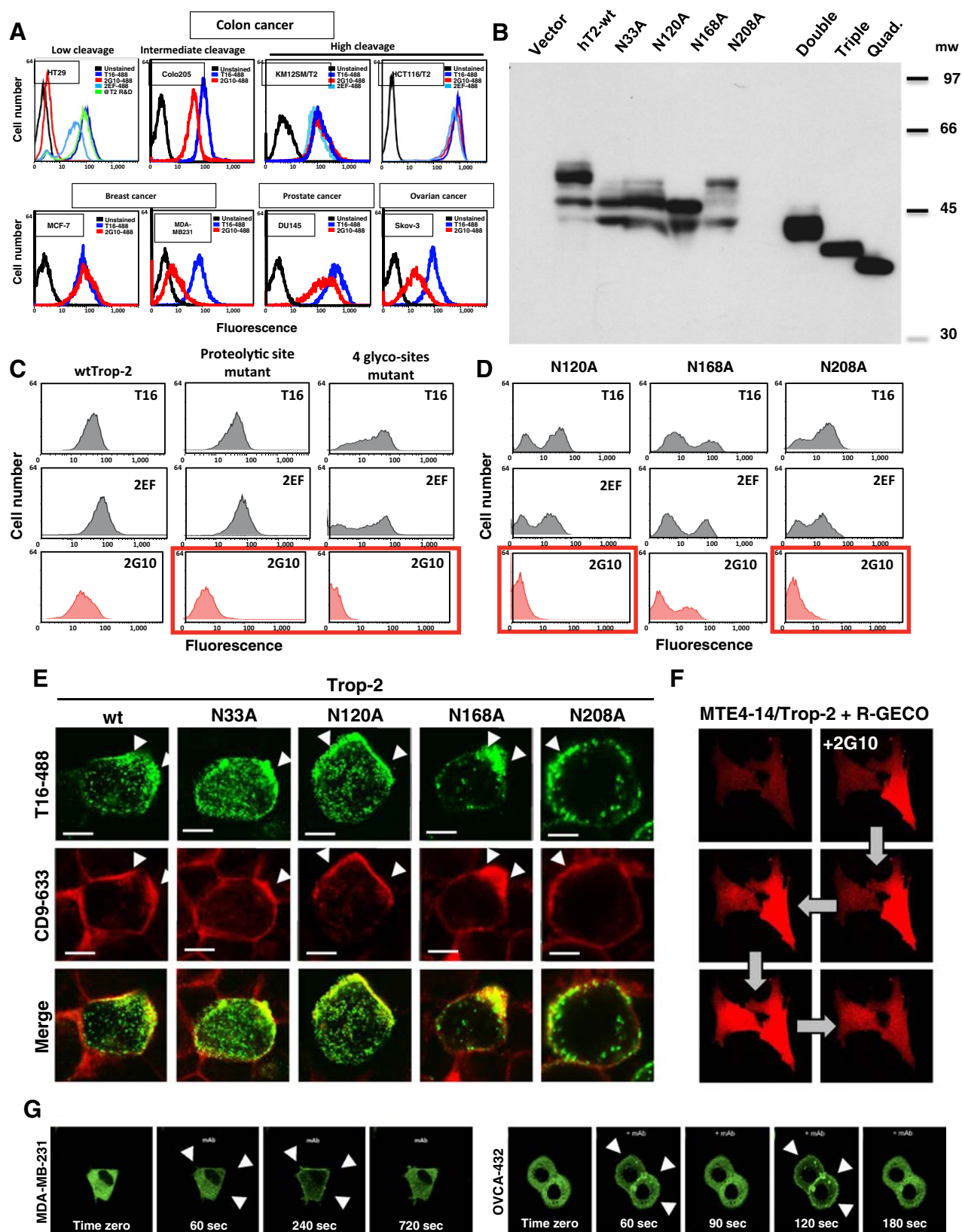


Figure 3.

Flow-cytometry analysis of ELISA-selected anti-Trop-2 mAb. **A**, Living L/Trop-2 transfectants expressing native Trop-2 at the cell surface were incubated with the indicated mAb, followed by incubation with a donkey anti-mouse antiserum conjugated to Alexa-488 fluorophores (red profiles); L cells transfected with the empty vector were used to assess binding specificity (black profiles). The Alexa-488-tagged AbT16 anti-Trop-2 mAb (blue profile, top left) was used as benchmark. Five of 10 ELISA-selected mAbs were found to bind native Trop-2 in living cells in culture; their combined binding profiles are shown in the red-framed bottom-right panel. **B**, Differential recognition of different ECD regions of the Trop-2 molecule by the five selected anti-Trop-2 mAbs. Trop-2 binding mAbs for each ECD region are indicated (red circles). **C**, Cross-competition of the five selected anti-Trop-2 mAbs. Flow-cytometry analysis of L/Trop-2 transfectants stained with Alexa-488-tagged mAbs (magenta profiles) either alone (top row) or competed out by a 10-fold excess of unlabeled mAbs. Each mAb (columns) was tested against itself (red frames) or against each one of the remaining mAbs, in pairwise combinations. A reduction of the fluorescence signals indicates that the two antibodies compete for the same epitope on the Trop-2 molecule. Unstained controls are shown in black-line profiles.



of the breast ($n = 1,701$), colon/rectum ($n = 413$), stomach ($n = 82$), endometrium ($n = 25$), lung ($n = 86$), ovary ($n = 79$), prostate ($n = 75$), pancreas ($n = 40$), cervix ($n = 35$), kidney ($n = 17$), thyroid ($n = 140$), skin ($n = 55$), pulmonary carcinoid ($n = 39$), and thymic epithelial tumors ($n = 193$) showed percent positivity for Trop-2 in up to 91% of individual cases (cervix), supporting Trop-2 as a major target in human cancer (12, 14, 16, 45). Lymphomas, melanomas, glioblastomas, and sarcomas did not express the Trop-2 protein (Fig. 1A and B).

These findings lent support to using Trop-2 as a main candidate for targeted anticancer therapy (46). We and others, though, had shown that Trop-2 is highly expressed in several normal tissues (9, 12, 14, 16, 17, 45), including epidermis, endometrium, esophagus, tonsil, lung, kidney, salivary glands, and breast (9). Importantly, the Rinat-Pfizer RN926 anti-Trop-2 mAb, which was developed in the PF-06664178/Aur0101 ADC, showed high efficacy in animal models that did not express human Trop-2. Follow-up studies in clinical settings showed, however, intolerable skin rash and mucosal lesions, as on-target/off-cancer toxicity due to the expression of Trop-2 in these tissues (25). This confirmed that toxicity of a highly potent ADC via on-target/off-cancer effects can be an unsurmountable limiting factor for effective use as anticancer therapy (47).

We thus set out to reach differential recognition of Trop-2 in transformed versus normal tissues. Trop-2 molecules form stable dimers (35) and higher-order multimers at cell-cell contacts (24, 48). Hence, target epitopes at different sites in Trop-2 may become differentially accessible to antibody binding in difficult-to-penetrate, tightly packed cancer cell masses. We thus performed initial screening assays on isolated cells and validated their performance on frozen sections of *in vivo* growing xenotransplants.

We recently showed that Trop-2 undergoes ADAM10-mediated proteolytic cleavage between residues R87 and T88, in the first loop of its thyroglobulin domain. This cleavage occurs in most tumors, including colon, breast, prostate cancers, whereas no Trop-2 cleavage was detected in normal human tissues (14, 16). Proteolysis of Trop-2 at R87-T88 triggers cancer cell growth and metastatic diffusion, via inhibition of E-cadherin-mediated cell-cell adhesion (14, 16).

We thus constructed models of 3D structures of the Trop-2 ECD (www.rcsb.org/) to inform mAb selection. The initial human Trop-2 homology models (14) were validated on the crystal structures of Trop-2 (Fig. 1C and D). The N-terminal small subunit, which is severed from Trop-2 by ADAM10 cleavage at R87-T88 (14) was found to possess a quasi-pyramidal shape, its base made by

residues belonging to the S71-S81 α -helix. Two β -strands (T42-S45, Q54-A57) elevate from this basis and are topped by a short orthogonal α -helix. The interface between the cleaved N-terminal small subunit and the groove amounts to about $1,200 \text{ \AA}^2$, as measured by the PISA server, with residues involved in hydrogen bonds and salt bridges between the two opposing surfaces. ADAM10 cleavage is predicted to induce a profound rearrangement/opening up of the Trop-2 structure. The 27–87 AA subunit was modeled to move away from the transmembrane-anchored region, while remaining covalently bound to it via the Cys73-Cys108 disulfide bridge (Fig. 1C). Such displacement revealed an elongated groove (largely inaccessible previous to cleavage) containing the α -helix D218-K231 and the three loops G232-Q237, G102-F114, and V131-G132 (Fig. 1D).

Generation of mAbs recognizing cleaved/activated cancer-expressed Trop-2

We sought to generate anti-Trop-2 mAbs with selective reactivity against the groove region in cleaved/activated Trop-2 (Supplementary Methods). Most low-efficacy anti-Trop-2 mAbs recognize a single immunodominant epitope (14, 17, 19), which is poised between the N-terminal and the cysteine-free stem region at the end of the ECD (Fig. 2; ref. 1). Hence, we removed these regions by deletion mutagenesis, as previously described (19). These Trop-2 molecules lacking the immunodominant epitope were used for hybridoma screening and epitope region mapping (Fig. 2).

The Trop-2 groove region exposed by ADAM10 cleavage is flanked by the N208 and N120 glycosylation sites. Differential glycosylation of cell surface molecules is known to occur in cancer cells (49–51). Recognition of cancer antigens is frequently dependent on target protein glycosylation (49, 52), possibly through skewed immunization processes (50). Hence, to extend the target portfolio of cancer-selective Trop-2-binding mAb, we immunized mice with engineered target proteins expressing multi-phylo end-glycosylation patterns, which encompassed mammalian tumor cells (human 293 and murine L), baculovirus-expressing insect cells, yeast cells, and nonglycosylated protein-generated in *Escherichia coli* (Fig. 2).

Screening for cancer-specific anti-Trop-2 mAbs was performed by ELISA, bio-layer interferometry, flow cytometry, and fluorescence microscopy on cleaved/activated, WT and glycosylation site- or proteolytic site-mutagenized Trop-2 (Fig. 2). The specificity of the anti-Trop-2 mAb toward different ECD regions of the Trop-2 molecule was assessed by cell-based ELISA, using L cells transfected with Trop-2 deletion mutants. The top 10 Trop-2-binding hybridomas

Figure 4.

Glycosylation-dependent binding and signaling of 2G10. **A**, Flow-cytometry analysis of 2G10 binding to wtTrop-2 in colon cancer cell lines. HT29 cells show low Trop-2 cleavage; Colo-205 cells show low Trop-2 cleavage; HCT116 show high Trop-2 cleavage. Benchmark AbT16, 2EF anti-framework Trop-2 mAb and R&D anti-Trop-2 pAb were used to quantify Trop-2 molecules at the cell membrane. **B**, Western blot analysis of Trop-2 glycosylation mutants expressed in MTE 4–14 transfectants. Single mutants are indicated; combination mutants were obtained, whereby two, three, or all four (quad.) glycosylated asparagine residues were substituted with alanines. Vector: vector-alone, negative-control transfectant; wtTrop-2 transfectants: full-glycosylation control. mw: molecular weight markers are indicated on the right. **C**, Flow-cytometry analysis of KM12SM transfectants for 2G10 binding to (left) wtTrop-2, (middle) proteolysis-resistant mutant, (right) glycosylation-null Trop-2. Benchmark AbT16, 2EF anti-framework Trop-2 mAb were used to quantify Trop-2 molecules at the cell membrane. **D**, Flow-cytometry analysis of KM12SM transfectants for 2G10 binding to single glycosylation site Trop-2 mutants (N120A; N168A; N208A). Benchmark AbT16, 2EF anti-framework Trop-2 mAb were used to quantify Trop-2 molecules at the cell membrane. **E**, MTE 4–14 transfectants for wtTrop-2, N33A, N120A, N168A, N208A Trop-2 mutants were assessed for *in vivo* interactions at the cell membrane with CD9. Co-capping analysis was conducted, using the benchmark AbT16-Alexa488 anti-Trop-2 mAb and anti-CD9-Alexa633 mAb. IF analysis was performed in multiplex mode (Zeiss), whereby signals for each fluorophore were acquired independently. Co-caps of Trop-2 variants with CD9 are indicated by white arrowheads. Scale bars, $5 \mu\text{m}$. **F**, Anti-Trop-2 Hu2G10-induced Ca^{2+} signaling (representative frames extracted from the movie S1) MTE 4–14 cells transfected with Trop-2 and the GFP-based Ca^{2+} indicator CMV-G-GECO1.2 were subjected to cross-linking of Trop-2 with the Hu2G10 mAb, and transient peak of Ca^{2+} signaling was recorded. **G**, Dynamic analysis for membrane translocation of PKC α -EGFP chimeras was conducted on MDA-MB-231 breast cancer and OVCA-432 ovarian cancer transfectants. Frames from confocal-microscopy recorded movies are shown at time zero and at 30 sec-intervals after Trop-2 cross-linking with Hu2G10. Signaling showed expected kinetics, with a lag time ≈ 30 sec, peak signaling at 60 to 240 seconds and signal waning at >720 seconds in MDA-MB-231 (9). In OVCA-432, PKC α -EGFP membrane signals were shown to oscillate with a period of 30 to 60 seconds, before waning after 600 seconds.

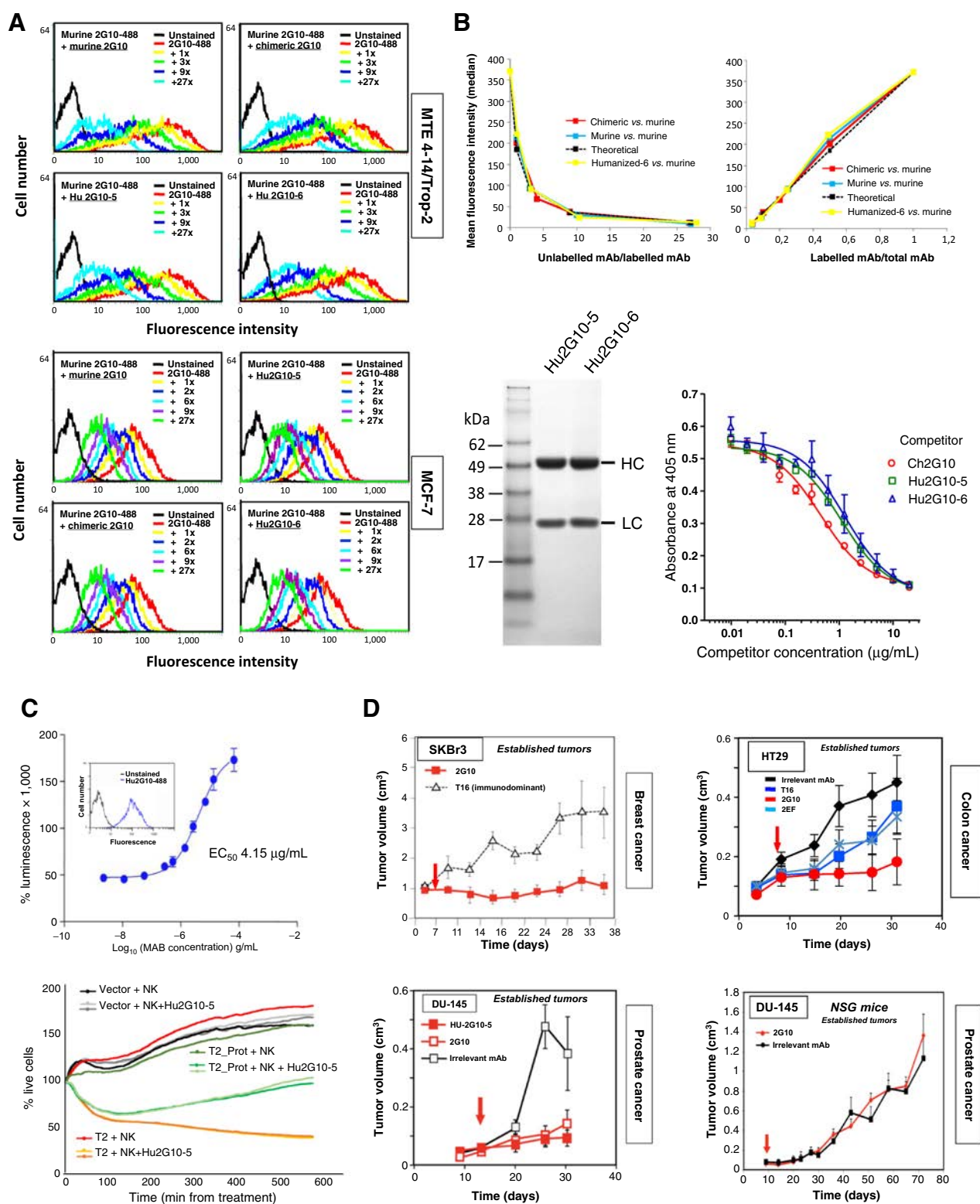


Figure 5. Hu2G10 engineering and immunotherapy of Trop-2-expressing cancer xenografts. **A**, Flow-cytometry analysis of MTE 4-14/Trop-2 transfectants (top) and MCF-7 breast cancer cells stained with Alexa-488-labeled murine 2G10 mAb either alone (red) or competed out by progressively higher amounts of the indicated mAb (murine 2G10, Ch2G10, Hu2G10-5, and Hu2G10-6). A reduction of fluorescence signal was a quantitative indicator of relative affinity, as the antibody pairs compete for the same epitope of the Trop-2 molecule. Unstained controls are shown in black. (Continued on the following page.)

were selected and further assessed by live cancer cell recognition by flow cytometry. Five of the 10 mAbs had the capacity to bind Trop-2 at the cell surface under native conditions (Fig. 3A and B). The specific reactivity of these mAbs was assessed by competition assays using pairwise combinations of fluorophore-tagged mAbs and a 10-fold excess of each of the other unlabeled mAb (Fig. 3C). These assays showed cross-competition of A9, 1B4, 2G10, 4F6 with each other, but not with 2EF. Together with the differential recognition of different ECD regions of the Trop-2 molecule (Fig. 3B), this suggested that two independent mAb families had been generated. Neither 2EF, nor the 2G10 family mAb cross-blocked the AbT16 and RS7 benchmark mAb, indicating no recognition of the immunodominant epitope in the Trop-2 ECD (Fig. 3B). Most effective recognition of the cleaved/activated form of Trop-2 by 2G10 led to its choice for prime development.

Structure-function determinants of the cleavage-activated, surface exposed, signal-triggering region of Trop-2

The 2G10 mAb was shown to bind Trop-2 in most cancer cell lines and transformed cell transfectants (Fig. 4A). The binding of 2G10 was shown to depend on Trop-2 proteolytic cleavage (Fig. 4C), first indicating success of our strategy in selective recognition of cancer cleaved/activated Trop-2 (14).

Four N-glycosylation site consensus sequences were identified in the Trop-2 protein, at N33, N120, N168, N208 (1, 53). Individual site N to A mutagenesis revealed that all four sites were glycosylated. Multiple-combination mutants were obtained until reaching a quadruple Trop-2 mutant that was completely devoid of glycosylation (Fig. 4B and C). All glycosylation mutants were found to be efficiently transported to the cell membrane. At the cell surface, individual glycosylation site mutants were shown to retain interaction with components of the macromolecular super-complex that drives Trop-2 signaling (9), among them CD9. Co-capping, upon mAb cross-linking, was shown for N33A, N120A, N168A, N208A Trop-2 with CD9 (Fig. 4E), suggesting conserved dynamic interaction with the Trop-2 signaling super-complex components and the cytoskeleton (9). This allowed the glycosylation site mutants to explore the glycan dependency of Trop-2 recognition by 2G10 in living cells.

Flow-cytometry analysis of quadruple glycosylation-site Trop-2 mutants showed effective recognition by the benchmark/immunodominant epitope-targeting AbT16 and by 2EF. On the other hand, 2G10 binding was entirely lost (Fig. 4C), indicating that the 2G10 target epitope is glycosylation-dependent. Individual glycosylation mutants were then assessed. The N33A and N168A mutants did not affect 2G10 binding, whereas N120A and N208A abolished it (Fig. 4D). This finding suggested recognition of the N120-N208-flanked activation-exposed Trop-2 groove. The region between the

N120 and N208 glycosylation sites was found to bind the cell-cell tight-junction instructor claudin-7 (53), and mutagenesis at these sites abolished claudin-7 binding (7, 53). These observations and the activation-linked exposure of this region suggested it as an initiator site of Trop-2 signaling.

We thus went on to ask whether the 2G10 mAb binding induced Trop-2 signaling *in vivo*. MTE 4–14 transfectants with the *TROP-2* gene and supertransfected with the R-GECO2 Ca²⁺-signal reporter were challenged with 2G10, and response was recorded by confocal time-lapse microscopy (Movie S1). A wave of Ca²⁺-signal was induced after binding of Trop-2 with the 2G10 mAb. In these assays, 2G10 and Hu2G10 showed undistinguishable activation profiles and were subsequently used interchangeably. Ca²⁺ signaling showed expected kinetics (8, 9) with a lag time of 10 seconds after mAb administration; peak signaling was reached after 30 seconds and waned after 30 additional seconds. This was followed by signal spreading to an adjoining cell (Fig. 4F), suggesting effective binding and modulation of Trop-2 function by 2G10. Endogenous Trop-2-expressing MDA-MB-231 breast cancer cells expressing the CMV-G-GECO1 responded to 2G10 mAb binding over corresponding time frames. The N-terminal ECD-targeting 2EF mAb did not induce calcium signaling.

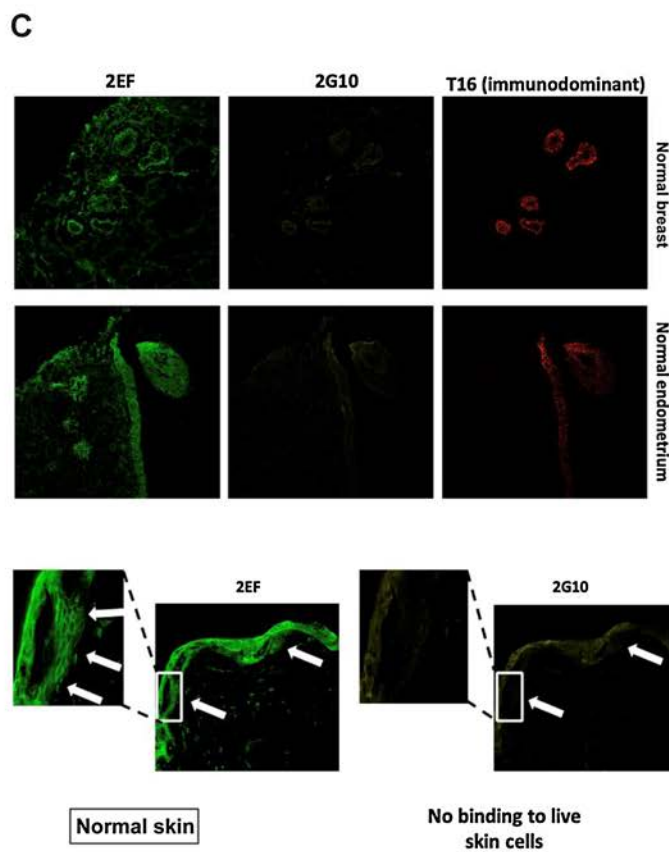
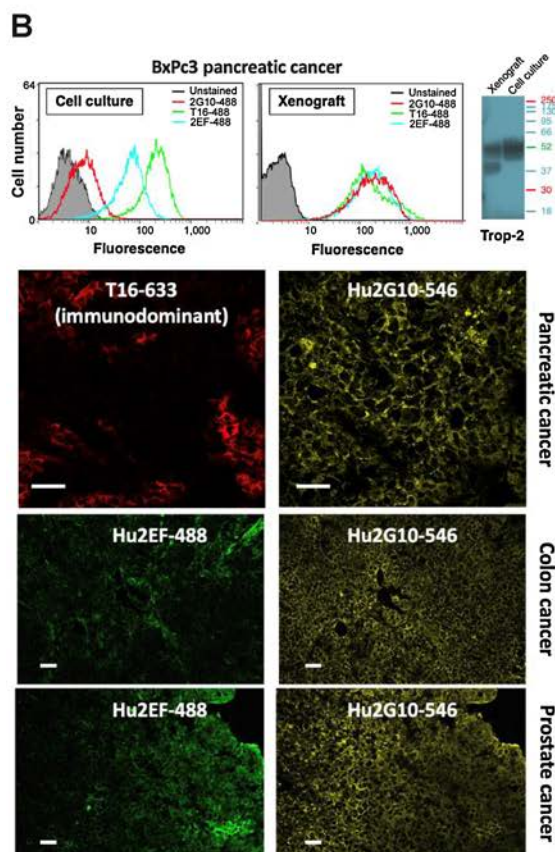
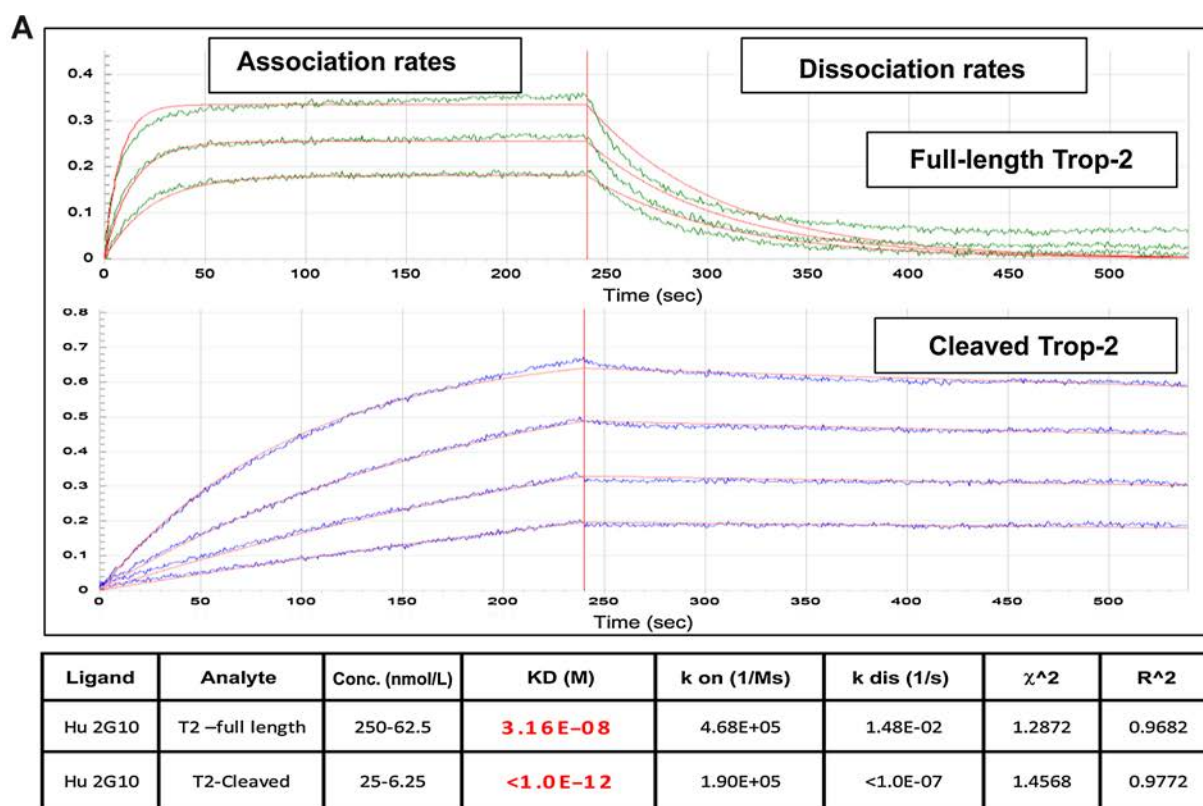
Activated PKC α is recruited to the cell membrane upon Ca²⁺ signaling (9). Western blot analysis showed dynamic modulation of phosphorylated/activated Ser657 PKC α and Ser473 AKT, after Trop-2 binding of 2G10, over 2- to 30-minute time frames (Supplementary Fig. S1). Absolute levels of AKT remained unvaried. Neither Ser657 PKC α nor Ser473 AKT phosphorylation were modulated by 2EF.

Dynamic analysis for membrane translocation of PKC α -EGFP chimeras (9) was conducted on MDA-MB-231 breast and OVCA-432 ovarian cancer cells. PKC α -EGFP signaling showed a lag time \approx 30 seconds, peak signaling at 60 to 240 seconds, and signal waning at $>$ 720 seconds in MDA-MB-231 (9). In OVCA-432, PKC α -EGFP membrane signals were found to oscillate with a period of 30 to 60 seconds, before waning after 600 seconds (9) (Fig. 4G). The 2EF mAb was found to induce no PKC α -EGFP translocation to the cell membrane.

Engineering of chimeric and humanized 2G10

To obtain mAbs that could be repeatedly administered to humans without eliciting a human anti-mouse antibody (HAMA) response, the 2G10 mAb was humanized. The first step was the construction of the chimeric 2G10 (Ch2G10), where the 2G10 VH and VL were grafted onto human G1 and κ constant regions. The CDR sequences of VH and VL were integrated into acceptor template human sequences, and subsequent rounds of single AA substitutions were carried out using their murine counterparts. These substitutions were based on 3D structure analysis, which predicted their importance in

(Continued.) **B**, Top, Data from the (A) panel were plotted as (left) ratio of unlabelled mAb/labelled mAb versus mean fluorescence intensity or as (right) labelled mAb/total mAb ratio versus mean fluorescence intensity. Theoretical curves are added in black for reference. Bottom left, PAGE analysis/Blue Coomassie staining of purified Hu2G10-5 and Hu2G10-5 produced in CHO cells transfectants, showing lack of contaminants and correct molecular weight of heavy (HC) and light (LC) chains. Molecular weight standards are indicated. Bottom, right, Competitive binding ELISA to characterize the affinity of Ch2G10, Hu2G10-5 and Hu2G10-6 to Trop-2-Fc. Binding of mouse 2G10 antibody in the presence of various concentrations of Ch2G10, Hu2G10-5, or Hu2G10-6 was analyzed. Absorbance values (Y-axis) are plotted at each antibody concentration tested (X-axis) in the figure. IC₅₀ values were calculated using GraphPad Prism. **C**, Hu2G10-mediated ADCC. Top, ADCC dose-response curve following incubation of subconfluent MCF-7 cells with serial dilutions of the Hu2G10 mAb and effector Jurkat NF-kB/NFAT-reporter cells. Luminescence data from the NF-kB/NFAT-reporter activation (three replica wells per data point) were plotted against mAb concentration, according to a 4-parameter logistic nonlinear regression model. The EC₅₀ was calculated using GraphPad Prism software. Error bars: \pm SEM. Inset: flow-cytometry analysis of Hu2G10 binding to target MCF-7 cells. Bottom, ADCC assessment using fresh human NK cells as effectors on target KMSM transfectant; impedance-based real-time analysis was used to measure target cell death. Cell density values (Y-axis) were normalized at time 0 (treatment administration) and plotted over time. Each treatment was performed in two replica wells, with measurements recorded every three minutes. **D**, Athymic nude or (bottom right) NSG mice were subcutaneously injected with human breast, colon, prostate cancer cells as indicated. Injected mice were randomized ($n = 16$ per group) and treated with 800- μ g mAb administered weekly until sacrifice. Treatment begun when tumors reached an average volume of 0.1 cm³ or at the time of tumor cell injection, as indicated (red arrow). Mice in the control groups received an irrelevant isotype-matched mAb. The AbT16 anti-Trop-2-immunodominant site mAb and 2EF was used as reference for anti-Trop-2 immunotherapy. Tumor volumes were plotted against time. Error bars: \pm SEM.



correctly forming the antigen-binding surface of the 2G10 monoclonal antibody. This process was aimed at enhancing the binding affinity toward the target (Fig. 5A). Two optimized humanized versions of the 2G10 antibody were selected: Hu2G10-5 and Hu2G10-6. These two versions differed by only one amino acid residue but had similar binding affinity to the target. Their binding affinity was marginally lower than the original mouse 2G10 antibody, known as Ch2G10, as determined by a competitive binding ELISA assay using Trop-2-Fc in the presence of murine 2G10 (Fig. 5B). These were then stably expressed in NS0 cells or CHO cells, and best producer CHO clones were isolated and used for mAb production *in vitro* (Fig. 5B).

Hu2G10 binding affinity

Hu2G10-5, Hu2G10-6, and CH2G10 mAb binding to native surface Trop-2 expressed by MTE 4-14 transfectants or MCF-7 breast cancer cells was assessed by flow cytometry, in competition assays with the murine 2G10. Most reassuring, this finding showed essentially unvaried binding abilities, with an IC_{50} value of 0.46 $\mu\text{g}/\text{mL}$ for Ch2G10, 1.1 $\mu\text{g}/\text{mL}$ for Hu2G10-5, and 1.3 $\mu\text{g}/\text{mL}$ for Hu2G10-6 (Fig. 5A and B).

Octet assays were then performed using Bio-Layer Interferometry for measuring absolute binding parameters of Hu2G10 to recombinant Trop-2, binding affinity constants and association/dissociation kinetics. Recombinant uncleaved Trop-2 was bound by Hu2G10 with a K_d of 3.16×10^{-8} mol/L. Hu2G10 binding to the fully cleaved recombinant Trop-2 showed a much tighter K_d of $<1.0 \times 10^{-12}$ mol/L (Fig. 6A). Hence, Hu2G10 binds ADAM10-cleaved, cancer-expressed Trop-2 >10,000 fold better than WT/normal cell Trop-2. The on- and off-binding kinetics of Hu2G10 for the uncleaved versus cleaved Trop-2 appeared vastly different. A most notable feature was the essentially nil dissociation rate of Hu2G10 once bound to the cleaved Trop-2 generated in cancer cells (Fig. 6A).

Trop-2 cleavage leads to hu2g10 binding to cancer cells *in vivo*

Cell confluency in culture was shown to heavily affect Trop-2 proteolysis in transformed cells (14), suggesting ADAM10 cleavage *in trans* from contacting cells. High cell density and persistent exposure to ADAM10 cleavage in tumors were thus predicted to increase Trop-2 cleavage *in vivo*. We comparatively analyzed BxPc3 pancreatic cancer cells for AbT16, 2EF and 2G10 binding in cell culture versus tumor xenotransplants (Fig. 6B). This showed a low fraction of cleaved Trop-2 and of Hu2G10 binding under 2D culture conditions. *In vivo* xenotransplanted BxPc3 cancer cells revealed much more extensive Trop-2 cleavage and Hu2G10 binding. Multiplex confocal microscopy IF analysis of BxPc3 pancreatic cancer xenografts showed much more extensive and prevalent Hu2G10 binding to cancer cells, as opposed to 2EF and to the immunodominant epitope-binding AbT16. Corresponding findings were obtained in the DU-145 prostate and KM12SM colon cancer

xenografts. This indicated not only high binding efficiency, but also much more efficient access to target Trop-2 cleavage sites in tumors (Fig. 6B). Parallel analysis of normal tissues showed no Trop-2 cleavage and no detectable binding of Hu2G10 to normal skin, breast, and endometrium (Fig. 6C).

ADCC by hu2g10

ADCC can mediate a large fraction of mAb anticancer effects (54). The ADCC potential of Hu2G10 mAb was measured using as effector Jurkat cells stably expressing the V158 (high affinity) Fc γ RIIIa receptor and an NFAT response element upstream of firefly luciferase. ADCC causes NFAT pathway activation with expression of the luciferase reporter gene, then quantified by a luminescence assay. MCF-7 breast cancer cells express endogenous Trop-2 at levels corresponding to average amounts in primary human cancers (12) and were used as target cells (Fig. 5C). Different amounts of purified mAb (range, 10^{-4} – 10^{-9} g/mL) were added to monolayers of MCF-7 target cells, together with Jurkat effector cells, at 3:1 effector/target cell ratios. The EC_{50} for the Hu2G10 mAb was 4.15 $\mu\text{g}/\text{mL}$ (2.96–5.83 $\mu\text{g}/\text{mL}$ 95% confidence interval).

We strengthened these findings by assessing the ADCC elicited by the Hu2G10 exploiting primary NK cells in PBMCs as effectors and measuring cell death as final outcome. Highly sensitive and specific real-time impedance-based measurement of cell death was employed (42) (Supplementary Fig. S2). Efficient ADCC-dependent killing was observed on target KM12SM/Trop-2 cells, while no killing was observed on the KM12SM/vector or in the absence of the antibody (Fig. 5C). We tested antibody specificity for the cleaved Trop-2 directly on the proteolytically impaired Trop-2 mutant. While initial killing was observed, after 2 hours, the cell population recovered and paralleled the control without mAbs (Fig. 5C). These results are consistent with differential binding of the Hu2G10 mAb to the cleaved versus uncleaved Trop-2. Initial killing suggests low background cleavage of WT-like proteolytically impaired Trop-2 mutant under the high cell density conditions of the assay.

Xenograft growth inhibition by hu2g10

The therapeutic efficacy of the Hu2G10 anti-Trop-2 mAb was tested *in vivo* against human cancer xenografts in nude mice. Xenograft-bearing mice ($n = 16$ per experimental group) were treated when tumors reached an average volume of 0.3 cm^3 at the time of mAb injection. Mice in the control group received an irrelevant isotype-matched mAb. AbT16, murine 2G10 and 2EF, AR47A6.4.2 and RS7, the parental antibody for SG/TRODELVY/IMMU-132 (21, 22), were used as benchmarks for the activity of Hu2G10 mAb.

Endotoxin-free Hu2G10 inhibited the growth of multiple Trop-2-expressing tumors, including prostate cancer (DU-145), colon cancer (HT29), and breast cancer (SKBr3; Fig. 5D). The anticancer activity of

Figure 6.

Hu2G10 recognition of cleaved/activated Trop-2 in cancer versus normal tissues. **A**, Affinity. Hu2G10 mAb absolute affinity was measured by Bio-Layer Interferometry-based label-free binding as described. Association/dissociation kinetics are shown for the proteolysis-resistant (top) and the fully cleaved (middle) Trop-2 ligands, plotted as wavelength shifts toward time with (association) or without (dissociation) analytes. Numerical values are shown from data fitting routines. Statistical analyses were conducted as described. **B**, Cancer cells. Top, Flow-cytometry analysis of BxPC3 pancreatic cancer cells growing *in vitro* or obtained by collagenase IV treatment of xenografts from nude mice with the Alexa488 2G10 or benchmark AbT16, 2EF anti-Trop-2 mAb. The same cells were subjected to Western blot analysis to assess the extent of Trop-2 cleavage *in vitro* versus *in vivo*. Bottom, Triple IF analysis of BxPc3 pancreatic, KM12SM colon, DU-145 prostate cancer xenografts. Frozen sections were incubated with a mixture of anti-Trop-2 antibodies directly labelled with distinct Alexa-fluorophores: 2EF-Alexa488, 2G10-Alexa546 and AbT16-Alexa633. IF analysis was performed in multiplex mode (Zeiss), whereby individual signals for each fluorophore were acquired independently, in a sequential manner. **C**, Normal cells. Triple IF analysis of normal breast, endometrium, skin. Frozen sections from normal tissues were stained and analyzed as above. Inset: detail of triple IF analysis of normal skin. The 2EF and the cancer-specific 2G10 signal is shown; white arrows indicate specific areas of Trop-2 expression, beneath the corneus layer.

Hu2G10 was undistinguishable from that of the murine 2G10, validating the reliability of the humanization procedure.

The 2G10 mAb was not able to reduce DU-145 xenotransplant growth in NGS mice (Fig. 5D, bottom right). NGS mice harbor a null mutation of the γ chain of the interleukin-2 receptor (IL2R γ) that blocks the signaling pathway for interleukins IL2, IL4, IL7, IL9, IL15, and IL21, thus resulting in the absence of functional NK cells. Also macrophages and dendritic cells are defective in these mice, due to alleles found in the NOD genetic background. Taken together with the corresponding efficacy in nude mice, and the ADCC activity measured *in vitro*, this suggests that mAb-driven ADCC is the main mechanism of Hu2G10 anticancer activity *in vivo*.

We did not observe any adverse effect in treated mice as compared with mice in the control group, as supported by normal behavior, clinical appearance and lack of variation in body weight during treatment (Supplementary Fig. S3).

The murine Trop-2 is not bound by 2G10 mAb (Supplementary Fig. S3). Hence, we went on to assay Hu2G10 toxicity in primates. Preliminary analysis of toxicity parameters in primates indicated normal clinical appearance and behavior together with lack of variation in body weight during treatment (Supplementary Fig. S3), supporting the safety of administration and the therapeutic potential of Hu2G10 against Trop-2-expressing tumors.

Discussion

Advanced, high-potency Trop-2-targeted therapy for metastatic cancer is urgently needed (27). However, next-generation approaches are hampered by expression of Trop-2 in normal tissues (9, 12, 14, 16, 17, 45), which can lead to unmanageable toxicity (25). We discovered that Trop-2 undergoes proteolytic activation by ADAM10 in cancer cells (14, 16). This exposes a previously inaccessible protein groove, flanked by two glycosylation sites. We designed a recognition strategy of such targets, for exploiting selective cancer vulnerability in patients. We succeeded in obtaining the 2G10 mAb family that selectively targets Trop-2-expressing cancer cells.

Our strategy design was informed by structure-function analysis of the Trop-2 ECD (14, 35). This led us to recognize that the N-terminal small subunit, which is severed from Trop-2 by ADAM10 cleavage at R87-T88 (14), masks a groove of the Trop-2 ECD and makes it largely inaccessible in the WT/uncleaved conformation. After ADAM10-mediated cleavage, the N-terminal small subunit only remains bound to the core Trop-2 structure via the Cys73-Cys108 disulphide bridge, and a profound rearrangement of the Trop-2 structure takes place, enabling targeting of the groove thus uncovered. Through selective immunization and screening strategies, we succeeded in generating the 2G10 mAb family that recognizes this region in an ADAM10 cleavage-dependent manner. The requirement for glycosylation at flanking sites supported the effective recognition of the cleavage-exposed target groove in Trop-2.

Trop-2 activation-site mutagenesis allowed to explore functional correlates, following transport to the cell surface and interaction with the macromolecular assembly that drives Trop-2 signaling (9). Trop-2 is required for the stability of the tight junction proteins claudin-7 and claudin-1, which are often dysregulated or lost in carcinogenesis. Trop-2 phosphorylation plays a role in the decrease or mislocalization of claudin-7. Furthermore, Trop-2 is phosphorylated at Ser-322 by PKC α (7, 9), and this phosphorylation enhances cell motility and decreases claudin-7 localization to

cellular borders (7). N120A and N208A Trop-2 mutagenesis showed that these glycan sites are critical for binding to claudin-7 (53). This and the selective modulation by 2G10 of Ca²⁺ signaling, AKT phosphorylation at Ser473, PKC α phosphorylation at Ser657, and the dynamic recruitment of PKC α at the cell membrane in cancer cells suggest that 2G10 targets a critical site for Trop-2 function. From a higher perspective, 2G10 thus appears to target the cancer-specific Trop-2 form, through recognition of the signal-trigger region for tumor progression and metastatic diffusion. This may provide selective pressure for association of the antibody with advanced and progressing cancers, for promising therapeutic applications in patients.

The Hu2G10 showed an extremely high affinity ($K_d < 1.0 \times 10^{-12}$ mol/L) for the cancer-specific, cleaved/activated Trop-2. Uncleaved wtTrop-2 was bound by Hu2G10 with a K_d of 3.16×10^{-8} mol/L, for a 10,000-fold lower affinity than for the cancer variety. For comparison, the K_d of HuRS7 is 1.2×10^{-9} mol/L (55), that is, RS7 has a $\approx 1,000$ lower affinity for Trop-2 than 2G10 and does not show differential recognition of normal versus transformed cells. Our findings of high differential binding to the Trop-2 tumor isoform by Hu2G10 and the absence of detectable binding of Hu2G10 to normal tissues, skin, breast, and endometrium, strongly support the potential for a high therapeutic index of Hu2G10 in patients.

Multiplex confocal microscopy analysis of BxPc3 pancreatic, DU-145 prostate, and KM12SM colon cancer xenografts showed much more extensive and prevalent Hu2G10 binding to cancer cells, as opposed to benchmark immunodominant epitope-binding mAb. This indicates not only high binding efficiency, but also much more efficient access to Trop-2 target sites in tumors. Consistently, Hu2G10 showed a powerful antitumor activity in multiple Trop-2-expressing preclinical tumor models, including prostate cancer (DU-145), colon cancer (HT29), breast cancer (SKBr3).

Recent findings support Hu2G10 as a strong candidate for next-generation ADC (29, 30), for enhanced selectivity and efficiency of payload delivery into tumor cells, while reducing the systemic toxicity caused by binding of normal cells. The lack of Hu2G10 toxicity in *in vivo* animal models and the selective recognition of cleaved/activated Trop-2 in cancer cells pave the way for a Hu2G10 mAb-led paradigm shift in Trop-2-targeted therapy.

Authors' Disclosures

E. Guerra reports personal fees and nonfinancial support from Oncoxx Biotech Srl; nonfinancial support from Mediterranea Theranostic Srl during the conduct of the study; nonfinancial support from Oncoxx Biotech Srl; nonfinancial support from Mediterranea Theranostic Srl outside the submitted work; has a patent for "Humanized anti-Trop-2 monoclonal antibodies and uses thereof" (WO2016087651) licensed to LegoChemBiosciences; and a patent for "Use of circulating serum Trop-2 as new tumor biomarker" (WO2017084763) issued. M. Trerotola reports a patent for WO2017/084763A1 issued to Saverio Alberti. S. Alberti reports personal fees and other support from Oncoxx Biotech srl; nonfinancial support and other support from Mediterranea Theranostic srl during the conduct of the study; personal fees and nonfinancial support from Oncoxx Biotech srl; nonfinancial support from Mediterranea Theranostic srl outside the submitted work; has a patent for "Humanized anti-Trop-2 monoclonal antibodies and uses thereof" (WO2016087651) licensed to LegoChemBiosciences; and a patent for "Use of circulating serum Trop-2 as new tumor biomarker" (WO2017084763) issued. No disclosures were reported by the other authors.

Authors' Contributions

E. Guerra: Conceptualization, data curation, formal analysis, supervision, validation, investigation, writing—original draft, writing—review and editing. **M. Trerotola:** Data curation, supervision, validation, investigation, writing—

original draft, writing–review and editing. **V. Relli:** Data curation, validation, investigation, visualization, writing–review and editing. **R. Lattanzio:** Data curation, formal analysis, validation, investigation, visualization, methodology, writing–review and editing. **R. Tripaldi:** Data curation, validation, investigation, visualization, methodology, writing–review and editing. **M. Ceci:** Data curation, validation, investigation, writing–review and editing. **K. Boujnah:** Data curation, formal analysis, supervision, validation, investigation, writing–review and editing. **L. Pantalone:** Investigation, methodology, writing–review and editing. **A. Sacchetti:** Data curation, formal analysis, validation, investigation, visualization, methodology, writing–review and editing. **K.M. Havas:** Data curation, validation, investigation, writing–review and editing. **P. Simeone:** Data curation, formal analysis, validation, investigation, visualization, writing–review and editing. **N. Travali:** Data curation, formal analysis, validation, visualization, writing–review and editing. **P. Querzoli:** Data curation, formal analysis, visualization, methodology, writing–review and editing. **M. Pedriali:** Data curation, formal analysis, validation, investigation, visualization, writing–review and editing. **P. Roversi:** Data curation, formal analysis, validation, methodology, writing–review and editing. **M. Iezzi:** Data curation, formal analysis, validation, investigation, writing–review and editing. **N. Tinari:** Resources, data curation, validation, visualization, writing–review and editing. **L. Antolini:** Conceptualization, data curation, formal analysis, investigation, visualization, methodology, writing–review and editing. **S. Alberti:** Conceptualization, formal analysis, supervision, funding acquisition, writing–review and editing.

References

- Fornaro M, Dell'Arciprete R, Stella M, Bucci C, Nutini M, Capri MG, et al. Cloning of the gene encoding TROP-2, a cell-surface glycoprotein expressed by human carcinomas. *Int J Cancer* 1995;62:610–8.
- Linnenbach AJ, Seng BA, Wu S, Robbins S, Scollon M, Pyrc JJ, et al. Retroposition in a family of carcinoma-associated antigen genes. *Mol Cell Biol* 1993;13:1507–15.
- Calabrese G, Crescenzi C, Morizio E, Palka G, Guerra E, Alberti S. Assignment of TACSTD1 (alias TROP1, M4S1) to human chromosome 2p21 and refinement of mapping of TACSTD2 (alias TROP-2, M1S1) to human chromosome 1p32 by in situ hybridization. *Cytogenet Cell Genet* 2001;92:164–5.
- Zanna P, Trerotola M, Vacca G, Bonasera V, Palombo B, Guerra E, et al. Trop-1 are conserved growth stimulatory molecules that mark early stages of tumor progression. *Cancer* 2007;110:452–64.
- Ciccarelli F, Acciarito A, Alberti S. Large and diverse numbers of human diseases with HIKE mutations. *Hum Mol Genet* 2000;9:1001–7.
- Basu A, Goldenberg DM, Stein R. The epithelial/carcinoma antigen EGP-1, recognized by monoclonal antibody RS7–3G11, is phosphorylated on serine 303. *Int J Cancer* 1995;62:472–9.
- Mori Y, Akita K, Ojima K, Iwamoto S, Yamashita T, Morii E, et al. Trophoblast cell surface antigen 2 (Trop-2) phosphorylation by protein kinase C alpha/delta (PKCalpha/delta) enhances cell motility. *J Biol Chem* 2019;294:11513–24.
- Ripani E, Sacchetti A, Corda D, Alberti S. The human Trop-2 is a tumor-associated calcium signal transducer. *Int J Cancer* 1998;76:671–6.
- Guerra E, Relli V, Ceci M, Tripaldi R, Simeone P, Aloisi AL, et al. Trop-2, Na⁺/K⁺ ATPase, CD9, PKC α , cofilin assemble a membrane signaling super-complex that drives colorectal cancer growth and invasion. *Oncogene* 2022;41:1795–808.
- Guerra E, Trerotola M, Tripaldi R, Aloisi AL, Simeone P, Sacchetti A, et al. Trop-2 induces tumor growth through Akt and determines sensitivity to Akt inhibitors. *Clin Cancer Res* 2016;22:4197–205.
- Stoyanova T, Goldstein AS, Cai H, Drake JM, Huang J, Witte ON. Regulated proteolysis of Trop-2 drives epithelial hyperplasia and stem cell self-renewal via beta-catenin signaling. *Genes Dev* 2012;26:2271–85.
- Trerotola M, Cantanelli P, Guerra E, Tripaldi R, Aloisi AL, Bonasera V, et al. Upregulation of Trop-2 quantitatively stimulates human cancer growth. *Oncogene* 2013;32:222–33.
- Trerotola M, Jernigan D, Liu Q, Siddiqui J, Fatatis A, Languino L. Trop-2 promotes prostate cancer metastasis by modulating β 1 integrin functions. *Cancer Res* 2013;73:3155–67.
- Trerotola M, Guerra E, Ali Z, Aloisi AL, Ceci M, Simeone P, et al. Trop-2 cleavage by ADAM10 is an activator switch for cancer growth and metastasis. *Neoplasia* 2021;23:415–28.
- Relli V, Trerotola M, Guerra E, Alberti S. Distinct lung cancer subtypes associate to distinct drivers of tumor progression. *Oncotarget* 2018;9:35528–40.

Acknowledgments

We thank the students and colleagues who supported us during the course of this work, through enduring discussion, advice and technical assistance. The support of Oncocx Biotech, of Mediterranea Theranostic, of FIRA – Finanziaria Regionale Abruzzese, of the Italian Ministry of Health (RicOncol RF-EMR-2006–361866), of the Italian Ministry of Development (FESR 2016–2018. SSI000651, art. 69 Reg. CE n. 1083/2006 and Reg. CE n. 1828/2006), of Region Abruzzo (POR FESR 2007–2013: Activity 1.1.1 line B, C78C14000100005), and of the Programma Per Giovani Ricercatori “Rita Levi Montalcini,” Italian Ministry of University and Research (Grant PGR12I7N1Z) to M. Trerotola is gratefully acknowledged.

The publication costs of this article were defrayed in part by the payment of publication fees. Therefore, and solely to indicate this fact, this article is hereby marked “advertisement” in accordance with 18 USC section 1734.

Note

Supplementary data for this article are available at Molecular Cancer Therapeutics Online (<http://mct.aacrjournals.org/>).

Received May 18, 2022; revised October 12, 2022; accepted March 13, 2023; published first March 15, 2023.

- Guerra E, Trerotola M, Relli V, Lattanzio R, Tripaldi R, Vacca G, et al. Trop-2 induces ADAM10-mediated cleavage of E-cadherin and drives EMT-less metastasis in colon cancer. *Neoplasia* 2021;23:898–911.
- Alberti S, Miotti S, Stella M, Klein CE, Fornaro M, Ménard S, et al. Biochemical characterization of Trop-2, a cell surface molecule expressed by human carcinomas: formal proof that the monoclonal antibodies T16 and MOv-16 recognize Trop-2. *Hybridoma* 1992;11:539–5.
- Truong AHL, Feng N, Sayegh D, Mak BC, O'Reilly K, Fung SW, et al. AR47A6.4.2, a functional naked monoclonal antibody targeting Trop-2, demonstrates in vivo efficacy in human pancreatic, colon, breast and prostate cancer models. *Mol Cancer Ther* 2007;6:3334s–s.
- Ikeda M, Yamaguchi M, Kato K, Nakamura K, Shiina S, Ichikawa-Ando T, et al. Pr1E11, a novel anti-TROP-2 antibody isolated by adenovirus-based antibody screening, recognizes a unique epitope. *Biochem Biophys Res Commun* 2015; 458:877–82.
- Guerra E, Alberti S. The anti-Trop-2 antibody-drug conjugate Sacituzumab Govitecan—effectiveness, pitfalls and promises. *Ann Transl Med* 2022;10:501–5.
- Bardia A, Mayer IA, Vahdat LT, Tolanev SM, Isakoff SJ, Diamond JR, et al. Sacituzumab govitecan-hziy in refractory metastatic triple-negative breast cancer. *N Engl J Med* 2019;380:741–51.
- Bardia A, Hurvitz SA, Tolanev SM, Loirat D, Punie K, Oliveira M, et al. Sacituzumab govitecan in metastatic triple-negative breast cancer. *N Engl J Med* 2021;384:1529–41.
- Tagawa ST. TROPHY-U-01: a phase II open-label study of sacituzumab govitecan in patients with metastatic urothelial carcinoma progressing after platinum-based chemotherapy and checkpoint inhibitors. *J Clin Oncol* 2021;39: 2474–85.
- Sun M, Zhang H, Jiang M, Chai Y, Qi J, Gao GF, et al. Structural insights into the cis and trans assembly of human trophoblast cell surface antigen 2. *iScience* 2021; 24:103190.
- King GT, Eaton KD, Beagle BR, Zopf CJ, Wong GY, Krupka HI, et al. A phase 1, dose-escalation study of PF-06664178, an anti-Trop-2/Aur0101 antibody-drug conjugate in patients with advanced or metastatic solid tumors. *Invest New Drugs* 2018;36:836–47.
- Ocean AJ, Starodub AN, Bardia A, Vahdat LT, Isakoff SJ, Guarino M, et al. Sacituzumab govitecan (IMMU-132), an anti-Trop-2-SN-38 antibody–drug conjugate for the treatment of diverse epithelial cancers: Safety and pharmacokinetics. *Cancer* 2017;123:3843–54.
- Okajima D, Yasuda S, Maejima T, Karibe T, Sakurai K, Aida T, et al. Datopotamab deruxtecan, a novel TROP-2-directed antibody–drug conjugate, demonstrates potent antitumor activity by efficient drug delivery to tumor cells. *Mol Cancer Ther* 2021;20:2329.
- Trerotola M, Guerra E, Alberti S. Letter to the editor: efficacy and safety of anti-Trop antibodies. *Biochim Biophys Acta* 2010;1805:119–20.

29. Kim H, Guerra E, Baek E, Jeong Y, You H, Yu B, et al. LCB84, a TROP-2–targeted ADC, for treatment of solid tumors that express TROP-2 using the hu2G10 tumor-selective anti-TROP-2 monoclonal antibody, a proprietary site-directed conjugation technology and plasma-stable tumor-selective linker chemistry. *Cancer Res* 2022;82:328.
30. Alberti S, Trerotola M, Guerra E. The Hu2G10 tumor-selective anti-Trop-2 monoclonal antibody targets the cleaved-activated Trop-2 and shows therapeutic efficacy against multiple human cancers. *Cancer Res* 2022;82:340.
31. Guncar G, Pungercic G, Klemencic I, Turk V, Turk D. Crystal structure of MHC class II-associated p41 Ii fragment bound to cathepsin L reveals the structural basis for differentiation between cathepsins L and S. *EMBO J* 1999;18:793–803.
32. Pavsic M, Guncar G, Djinovic-Carugo K, Lenarcic B. Crystal structure and its bearing towards an understanding of key biological functions of EpCAM. *Nat Commun* 2014;5:4764.
33. Nadezhdin KD, García-Carpio I, Goncharuk SA, Mineev KS, Arseniev AS, Vilar M. Structural basis of p75 transmembrane domain dimerization. *J Biol Chem* 2016;291:12346–57.
34. Pavsic M, Ilc G, Vidmar T, Plavec J, Lenarcic B. The cytosolic tail of the tumor marker protein Trop-2: a structural switch triggered by phosphorylation. *Sci Rep* 2015;5:10324.
35. Pavsic M. Trop-2 forms a stable dimer with significant structural differences within the membrane-distal region as compared to EpCAM. *Int J Mol Sci* 2021; 22:10640.
36. Lütteke T, Bohne-Lang A, Loss A, Goetz T, Frank M, von der Lieth CW. GLYCOSCIENCES.de: an Internet portal to support glycomics and glycobiology research. *Glycobiology* 2006;16:71r–81r.
37. Alberti S, Nutini M, Herzenberg LA. DNA methylation prevents the amplification of TROP1, a tumor associated cell surface antigen gene. *Proc Natl Acad Sci USA* 1994;91:5833–7.
38. Dell'Arciprete R, Stella M, Fornaro M, Ciccocioppo R, Capri MG, Naglieri AM, et al. High-efficiency expression gene cloning by flow cytometry. *J Histochem Cytochem* 1996;44:629–40.
39. Alberti S, Bucci C, Fornaro M, Robotti A, Stella M. Immunofluorescence analysis in flow cytometry: better selection of antibody-labeled cells after fluorescence overcompensation in the red channel. *J Histochem Cytochem* 1991;39:701–6.
40. Alberti S, Parks DR, Herzenberg LA. A single laser method for subtraction of cell autofluorescence in flow cytometry. *Cytometry* 1987;8:114–9.
41. Alberti S, Herzenberg LA. DNA methylation prevents transfection of genes for specific surface antigens. *Proc Natl Acad Sci USA* 1988;85:8391–4.
42. Tóth G, Szöllősi J, Vereb G. Quantitating ADCC against adherent cells: Impedance-based detection is superior to release, membrane permeability, or caspase activation assays in resolving antibody dose response. *Cytometry A* 2017; 91:1021–9.
43. Ambrogi F, Fornili M, Boracchi P, Trerotola M, Relli V, Simeone P, et al. Trop-2 is a determinant of breast cancer survival. *PLoS One* 2014;9:e96993.
44. Rossi C, Di Lena A, La Sorda R, Lattanzio R, Antolini L, Patassini C, et al. Intestinal tumor chemoprevention with the antioxidant lipoic acid stimulates the growth of breast cancer. *Eur J Cancer* 2008;44:2696–704.
45. Stepan LP, Trueblood ES, Hale K, Babcook J, Borges L, Sutherland CL. Expression of Trop-2 cell surface glycoprotein in normal and tumor tissues: potential implications as a cancer therapeutic target. *J Histochem Cytochem* 2011;59:701–10.
46. Mangino G, Capri MG, Barnaba V, Alberti S. Presentation of native Trop-2 tumor antigens to human cytotoxic T lymphocytes by engineered antigen-presenting cells. *Int J Cancer* 2002;101:353–9.
47. Krop IE, Im S-A, Barrios C, Bonnefoi H, Gralow J, Toi M, et al. Trastuzumab emtansine plus pertuzumab versus taxane plus trastuzumab plus pertuzumab after anthracycline for high-risk human epidermal growth factor receptor 2–positive early breast cancer: the phase III KATLLIN study. *J Clin Oncol* 2021;40: 438–48.
48. Balzar M, Briaire-de Bruijn IH, Rees-Bakker HAM, Prins FA, Helfrich W, Leij LD, et al. Epidermal growth factor-like repeats mediate lateral and reciprocal interactions of Ep-CAM molecules in homophilic adhesions. *Mol Cell Biol* 2001; 21:2570–80.
49. Matsuki H, Yonezawa K, Obata K, Iwata K, Nakamura H, Okada Y, et al. Monoclonal antibodies with defined recognition sequences in the stem region of CD44: detection of differential glycosylation of CD44 between tumor and stromal cells in tissue. *Cancer Res* 2003;63:8278–83.
50. Tarp MA, Sorensen AL, Mandel U, Paulsen H, Burchell J, Taylor-Papadimitriou J, et al. Identification of a novel cancer-specific immunodominant glycopeptide epitope in the MUC1 tandem repeat. *Glycobiology* 2007;17: 197–209.
51. Pauli C, Munz M, Kieu C, Mack B, Breinl P, Wollenberg B, et al. Tumor-specific glycosylation of the carcinoma-associated epithelial cell adhesion molecule EpCAM in head and neck carcinomas. *Cancer Lett* 2003;193:25–32.
52. Tomita Y, Arakawa F, Yamamoto T, Kuwahara M, Watanabe R, Iwasaki H, et al. Molecular identification of a human carcinoma-associated glycoprotein antigen recognized by mouse monoclonal antibody FU-MK-1. *Jpn J Cancer Res* 2000;91: 231–8.
53. Kamble PR, Patkar SR, Breed AA, Pathak BR. N-glycosylation status of Trop-2 impacts its surface density, interaction with claudin-7 and exosomal release. *Arch Biochem Biophys* 2021;714:109084.
54. Jonjic N, Alberti S, Bernasconi S, Peri G, Jilek P, Anichini A, et al. Heterogeneous susceptibility of human melanoma clones to monocyte cytotoxicity: role of ICAM-1 defined by antibody blocking and gene transfer. *Eur J Immunol* 1992;22: 2255–60.
55. Cardillo TM, Govindan SV, Sharkey RM, Trisal P, Goldenberg DM. Humanized anti-Trop-2 IgG-SN-38 conjugate for effective treatment of diverse epithelial cancers: preclinical studies in human cancer xenograft models and monkeys. *Clin Cancer Res* 2011;17:3157–69.